JOURNAL OF MATERIALS SCIENCE 27 (1992) 5783–5788

Effect of shot peening on the residual stress distribution in two commercial titanium alloys

B. R. SRIDHAR, W. G. NAFDE
Gas Turbine Research Establishment, Bangalore 560 093, India
K. A. PADMANABHAN
Department of Metallurgical Engineering, Indian Institute of Technology, Madras 600 036, India

The residual stress distribution in two commercial titanium alloys, the near-alpha IMI-685 and the alpha–beta IMI-318, have been determined using the method of drilling holes for the machined and polished as well as the machined, polished and shot-peened conditions. The residual stresses were always compressive and their peak values for both alloys were similar. However, the stress distribution patterns were different and this could have implications for the fatigue behaviour of the alloys.

1. Introduction

The two titanium alloys, near-alpha IMI-685 (composition in wt %: Ti–6Al–5Zr–0.5 Mo–0.25 Si) and the alpha–beta alloy IMI-318 (Ti–6Al–4V) find applications in gas turbine engines. The present work was concerned with the residual stress distribution patterns present in these two alloys in the machined and polished, as well as the machined, polished and shot-peened conditions.

The residual stress distribution pattern obtained in a material depends on the manner of preparation of its surface. The microstructure and mechanical properties are also known to affect the magnitude and distribution of the residual stresses. Shot peening induces residual compressive stresses. The peening variables are peening pressure, duration and diameter and type of the shots used. Peening intensity is measured in terms of the arc height developed on Almen strips (made from a spring steel) when they are peened on one surface. For titanium alloys, glass-bead peening is more effective than steel-ball peening [1–6].

Residual stress measurement by drilling a hole and using a strain gauge rosette is well established (Fig. 1). Per cent strain relieved by drilling a hole is often represented as a function of the dimensionless parameter Z/D_0, where Z is the depth at which the residual stress is measured and D_0 is the hole diameter. For obtaining accurate results, drilling of flat-bottomed holes using specially dressed end mills is essential. To avoid thermal effects, particularly in titanium-alloys that have poor thermal conductivity, drilling in small increments at low speeds is often resorted to. When the distribution of residual stresses is non-uniform, analysis is carried out assuming the distribution to be uniform in the depth interval Z to $(Z + \Delta Z)$ [7–15].

2. Experimental and analytical procedures

From the test rings of forgings made of both the alloys IMI-685 and IMI-318, specimens of dimensions 50 mm × 15 mm × 5 mm were machined. The surfaces of the specimens were polished down to 500 grade SiC emery. Glass beads, 0.1–0.2 mm diameter, suspended in water at a known concentration, were forced through a nozzle at a pressure of 480 kPa on to the polished surfaces of the specimens for about 2–3 min. Using 0.79 mm thick N-type Almen strips, the intensity at saturation was determined to be an Almen arc height of 0.35 mm (35 N).

Specimens in the machined and polished as well as the machined, polished and short-peened conditions

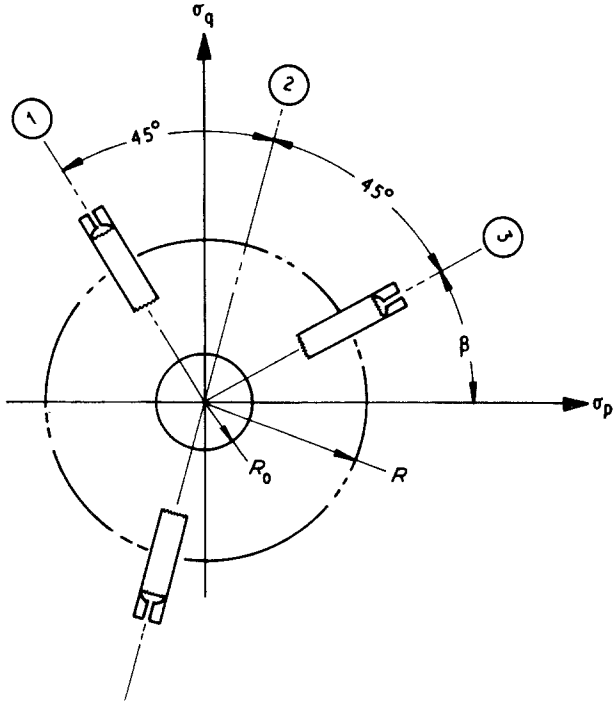

Figure 1 Strain gauge rosette arrangement for determining the residual stresses.

were rigidly fixed to a flat metallic base with araldite/dental cement. Strain gauge rosettes (EA-06-125RE-120, Micromeasurements) were bonded to the surface of specimens using cold-setting M-200 bonds. The strain gauges 1, 2 and 3 (Fig. 1) were connected to P-3500 strain indicator via a SB-10 switch and balance unit. All the strain gauges were initially balanced for null reading after adjusting the specified gauge factor (2.05 ± 1.00 %), the potentiometers of the SB-10 switch, and the balance unit.

Using an RS-200 milling guide (Fig. 2), the specimen was drilled in small increments of 25 μm down to a depth of 125 μm. Thereafter, the final depth was reached in steps of 125 μm. Following the recommendation of the manufacturer, drilling was restricted to a maximum depth of 0.5 D_o. The diameter of the hole was measured using a microscope that had a graduated eye piece. The depth was measured using a height gauge and related to the number of divisions of drilling marked on the micrometer of the milling gauge meant for the control of depth.

For each increment in depth, the readings from all three strain gauges were recorded. The strains relieved, ε_1, ε_2, and ε_3, were plotted as functions of the dimensionless parameter, Z/D_o.

The strain, $\varepsilon_i(Z)$, at the depth interval Z to $(Z + \Delta Z)$ is evaluated as

$$\varepsilon_i(Z) = (\Delta\varepsilon_i/p) \times 100 \quad (1)$$

where $\Delta\varepsilon_i[= \varepsilon_i(Z + \Delta Z) - \varepsilon_i(Z)]$ is the amount of strain relieved within a depth interval bounded by Z and $Z + \Delta Z$, as measured by a strain gauge i (= 1, 2 or 3); p is the corresponding per cent strain relieved as read from a Rendler–Vigness plot (per cent strain relieved versus Z/D_o for the case where the strain distribution is uniform [9]).

The principal residual stresses, σ_p and σ_q, at a depth Z are calculated from [10]

$$\sigma_p(Z) = \frac{M(Z)}{4A} + \frac{N(Z)}{4B\cos 2\beta} \quad (2)$$

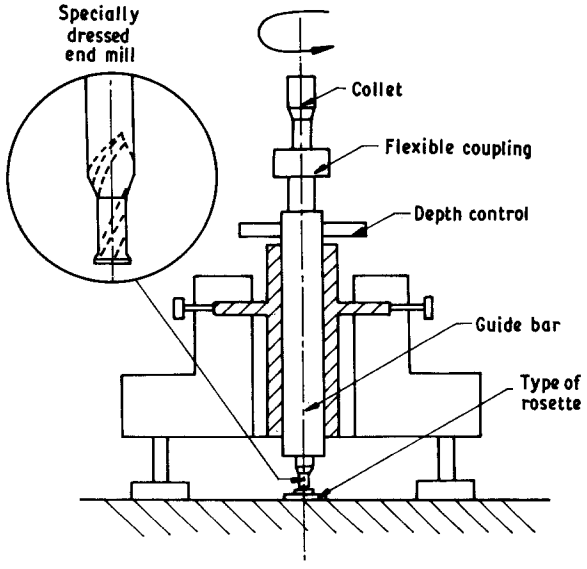

Figure 2 A schematic diagram of the milling guide.

and

$$\sigma_q(Z) = \frac{M(Z)}{4A} - \frac{N(Z)}{4B\cos 2\beta} \quad (3)$$

where $M(Z) = \varepsilon_3(Z) + \varepsilon_1(Z)$, $N(Z) = \varepsilon_3(Z) - \varepsilon_1(Z)$, $A = -(1 + \nu)/2Er^2$, $B = -(1 + \nu/2E)\{[4/(1 + \nu)r^2] - (3/r^4)\}$, with r = (gauge circle radius/hole radius) = (R/R_o), ν the Poisson's ratio and E the Young's modulus of the material. Tan 2β equals $[M(Z) - 2\varepsilon_2(Z)]/N(Z)$, where β is the angle the principal stress, σ_p, makes with the axis of strain gauge 3 at a depth Z.

The gauge circle radius of the rosette used here was 5.13 mm (given). The measured hole radius was 1.625 mm. Using appropriate values of the elastic constants, A and B were calculated, as follows to be:

IMI-685

$$4A = -2.14 \times 10^{-3}\,(\text{GPa})^{-1}$$

$$4B = -5.81248 \times 10^{-3}\,(\text{GPa})^{-1}$$

IMI-318

$$4A = -2.5386 \times 10^{-3}\,(\text{GPa})^{-1}$$

$$4B = -6.8030 \times 10^{-3}\,(\text{GPa})^{-1}$$

For reasons of symmetry and ease in the analysis of subsequent axial fatigue tests, it is convenient to work in terms of the residual stresses present along the longitudinal, σ_L, and transverse, σ_T, directions of the test specimen. Evidently,

$$\sigma_L = \sigma_p\cos\beta + \sigma_q\sin\beta \quad (4)$$

and

$$\sigma_T = \sigma_p\sin\beta - \sigma_q\cos\beta \quad (5)$$

3. Results and discussion

The microstructure of IMI-685 consisted of acicular (h c p) alpha in basket-weave form separated by thin layers of (b c c) beta (Fig. 3a). The microstructure of IMI-318 (Fig. 3b) was made up of equiaxed alpha with the beta phase being present at the alpha-phase boundaries.

3.1. Residual stresses in IMI-685

3.1.1. Machined and polished condition

The strains relieved, ε_1, ε_2 and ε_3, are shown in Fig. 4 as functions of Z/D_o. The relieved strains were all positive and they saturated with increasing depth below the surface. Fig. 5 is a plot of σ_p and σ_q (both compressive) as functions of depth below the surface. The peak value of σ_p (= −320 MPa) was present at the surface, while that of σ_q (= −320 MPa) was located at a depth of about 40 μm. Beyond this depth, the decay in both the stresses was nearly uniform. The magnitude and direction (indicated by the value of the angle β) of the principal residual stresses varied with depth. Fig. 6 shows σ_L and σ_T as functions of depth. They had their maximum value at the surface and σ_T was always greater than σ_L. The depth of the compressively stressed layer for this condition was about 0.45 mm.

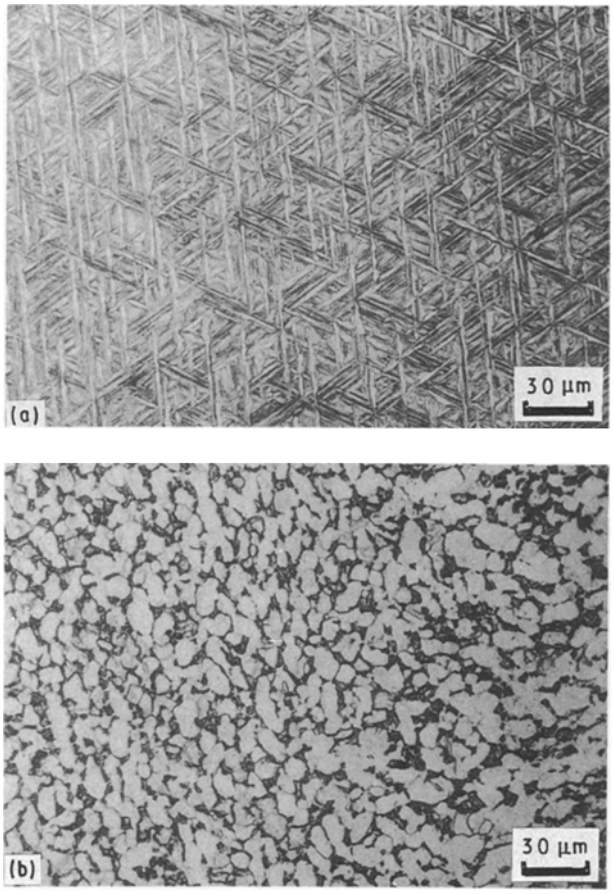

Figure 3 Optical micrographs of (a) as-received IMI-685 alloy showing acicular alpha (white features) separated by thin layers of beta (dark features), and (b) IMI-318 alloy showing equiaxed alpha with the beta phase at the alpha boundaries.

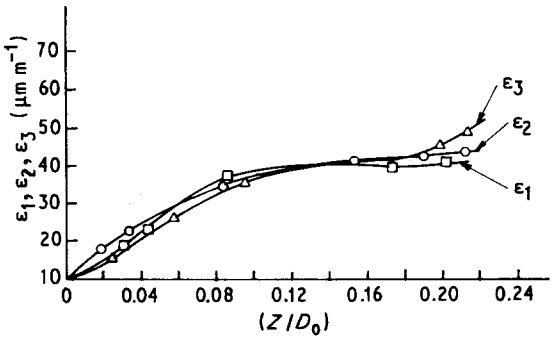

Figure 4 Variation of the strains relieved as functions of Z/D_o. IMI-685, machined and polished condition.

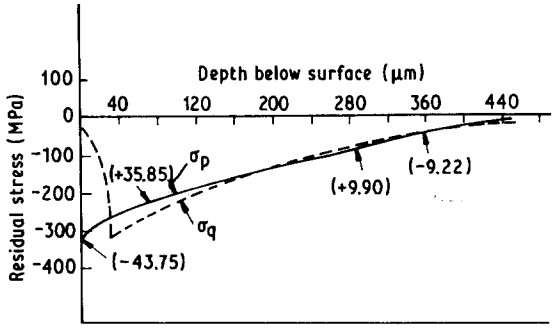

Figure 5 Variation of the principal residual stresses as functions of depth below the specimen surface. IMI-685, machined and polished condition. The figures in parentheses indicate the magnitude of the angle β (Fig. 1) in degrees.

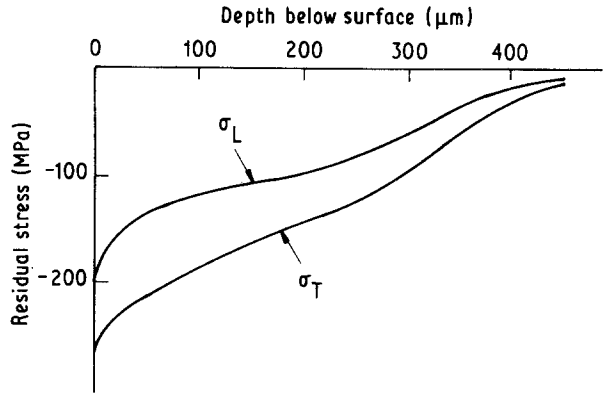

Figure 6 Variation of the longitudinal and transverse residual stresses as functions of depth below the specimen surface. IMI-685, machined and polished condition.

3.1.2. Machined, polished and shot-peened condition

Fig. 7 presents the strains relieved as functions of Z/D_o. Again, the relieved strains were all positive and tended to saturate with depth. But their magnitudes were significantly greater than those for the machined and polished condition. In Fig. 8, σ_p and σ_q (both compressive) are plotted as functions of depth below the surface. Their maxima were at the surface ($\sigma_{p,max} = -650$ MPa; $\sigma_{q,max} = -350$ MPa) and they decayed to zero with increasing depth. σ_p was greater than σ_q down to a depth of 0.15 mm, below which level the trend was reversed. As before, both the magnitude and direction of the principal residual stresses varied with depth. Fig. 9 shows the variation of the longitudinal and transverse residual stresses (both compressive) with depth below the surface. Here, σ_L was greater than σ_T practically over the entire compressively stressed layer, which was slightly in excess of 0.75 mm deep.

Shot peening had increased both the magnitudes of the residual compressive stresses and the depth of the stressed layer (cf. Figs 6 and 9). It has been suggested [5, 6] that the peak residual stresses present in a shot-peened material are about 50%–60% of its yield strength. The present peak value, σ_L, of -710 MPa works out roughly as 70% of the 0.2% proof stress of IMI-685 ($\sigma_{yield} = 1020$ MPa).

3.2. Residual stresses in IMI-318

3.2.1. Machined and polished condition

Fig. 10 presents the strains relieved as functions of Z/D_o. The curves are similar to those presented earlier. In Fig. 11, σ_p and σ_q (both compressive) are plotted as functions of depth below the surface. Their peak values ($\sigma_{p,max} = -380$ MPa, $\sigma_{q,max} = -200$ MPa) were found at a depth of about 60 μm. Always, σ_p was greater than σ_q but its magnitude and direction changed with depth. In Fig. 12, σ_L and σ_T (both compressive) are shown as functions of depth below the surface. Their peak values ($\sigma_L = -210$ MPa; $\sigma_T = -380$ MPa) were present at a depth of 60 μm and 35 μm respectively. Always, σ_T was greater than σ_L.

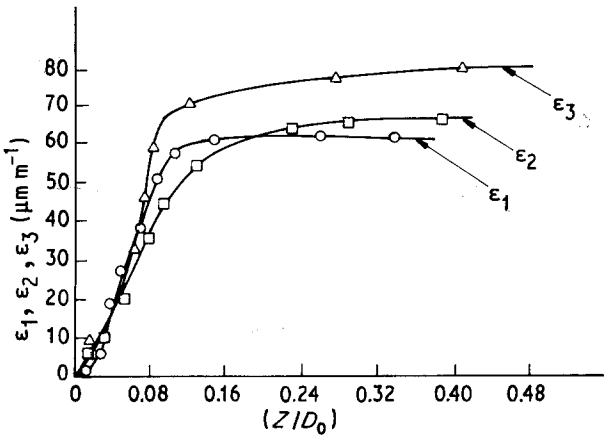

Figure 7 Variation of the strains relieved as functions of Z/D_o. IMI-685, machined, polished and wet-glass peened condition.

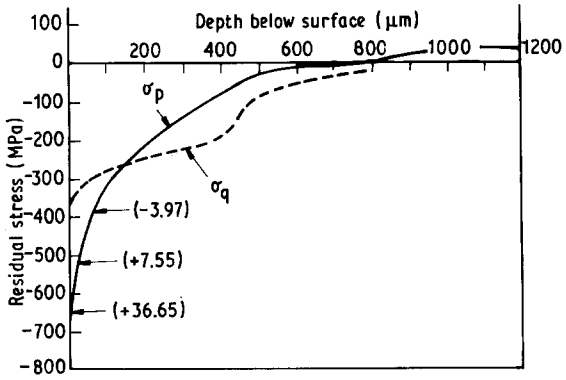

Figure 8 Variation of the principal residual stresses as functions of depth below the specimen surface. IMI-685, machined, polished and wet-glass peened condition. The figures in parentheses indicate the magnitude of the angle β in degrees.

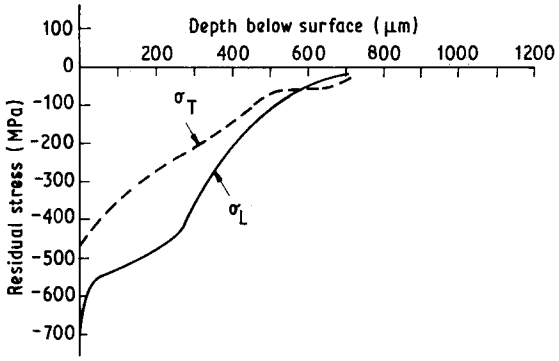

Figure 9 Variation of the longitudinal and transverse residual stresses as functions of depth below the specimen surface. IMI-685, machined, polished and wet-glass peened condition.

The depth of the stressed layer for this condition was about 0.14–0.15 mm.

3.2.2. Machined, polished and shot-peened condition

Fig. 13 shows the strains relieved (all positive and increasing with depth) as functions of Z/D_o. Their magnitudes were far greater than those present in material in the machined and polished condition. σ_p and σ_q (both compressive, with a nearly equal peak

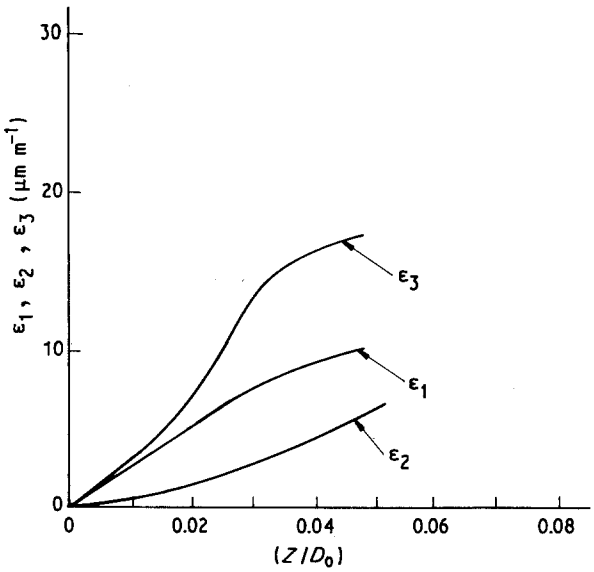

Figure 10 Variation of the strains relieved as functions of Z/D_o. IMI-318, machined and polished condition.

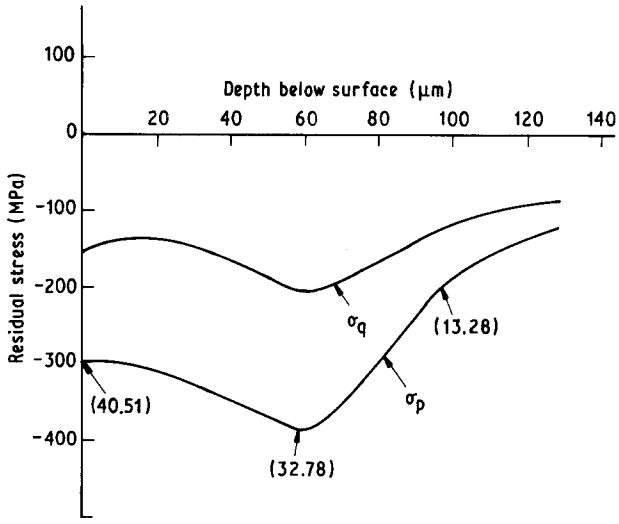

Figure 11 Variation of the principal residual stresses as functions of depth below the specimen surface. IMI-318, machined and polished condition. The figures in parentheses indicate the magnitude of the angle β in degrees.

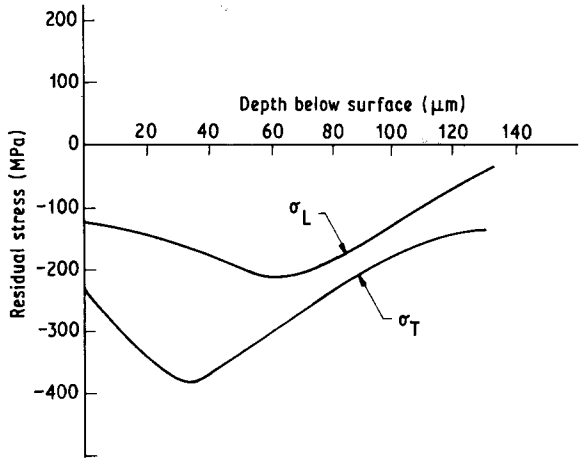

Figure 12 Variation of the longitudinal and transverse stresses as functions of depth below the specimen surface. IMI-318, machined and polished condition.

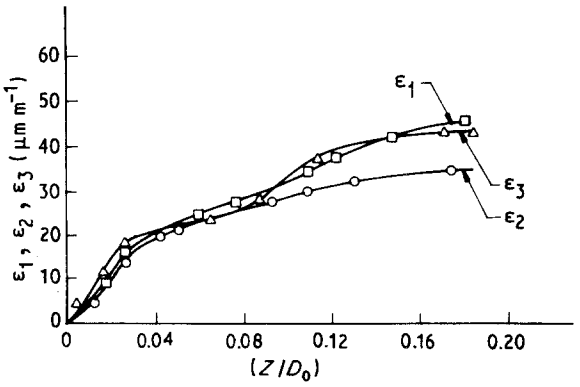

Figure 13 Variation of the strains relieved as functions of Z/D_o. IMI-318, machined, polished and wet-glass peened condition.

value of − 550 MPa) are plotted in Fig. 14 as functions of depth below the surface. The depth of the compressively stressed layer was about 0.83 mm, below which, for a small additional depth, small tensile components were present. Both the magnitude and direction of the principal stresses changed with depth. Fig. 15 shows plots of σ_L and σ_T (both compressive, with a nearly equal peak value of − 705 MPa at a depth of 25–30 μm) as functions of depth below the surface. The compressively stressed layer extended to a depth of 0.75 mm, below which small tensile components were found down to a total depth of 0.85 mm.

Shot peening significantly increased the depth of the stressed layer as well as the magnitudes of the residual compressive stresses (cf. Figs 12 and 15). The peak longitudinal residual stress (= − 705 MPa) was about 75% of the 0.2% proof stress of IMI-318 (σ_{yield} = 930–950 MPa).

3.3. Residual stress distribution in IMI-685 and IMI-318: a comparison

In the machined and polished condition, the stressed layer extended to a greater depth in IMI-685 than in IMI-318 (cf. Figs 6 and 12).

It has been reported that when the hardness is less than 300 HV, the maximum residual stress is present at the surface, but in medium hard and very hard materials, it is present in the sub-surface regions. However, lower shot diameters and higher shot velocities can cause the peak residual stress to shift from the sub-surface to the surface layers [16–19].

IMI-685 and IMI-318 have a hardness of about 350 HV. The sub-surface residual stress peak observed in IMI-318 is in agreement with the finding of Wohlfahrt [19] concerning materials of medium hardness. But the surface residual stress peaks seen in IMI-685 in both the machined and polished as well as the machined, polished and shot-peened conditions is contrary to the above result. Perhaps the difference can be traced to the difference in the work-hardening rates of the two materials. H c p metals (limited number of slip systems) display a lower strain-hardening rate than the cubic metals. Thus, the work-hardening rate of the near alpha (h c p) IMI-685 is likely to be lower than that of the alpha plus beta (b c c) IMI-318. (Rama Rao [20] has experimentally verified this.) Then, under a given intensity of shot peening, the surface layers of IMI-685 are expected to deform more than those of IMI-318. In such a situation, the peak residual stress in the former material is likely to be present at the surface, which is indeed the case.

A residual stress has an effect similar to that of an applied stress. As the residual stress distribution in the two alloys was different, shot peening may influence

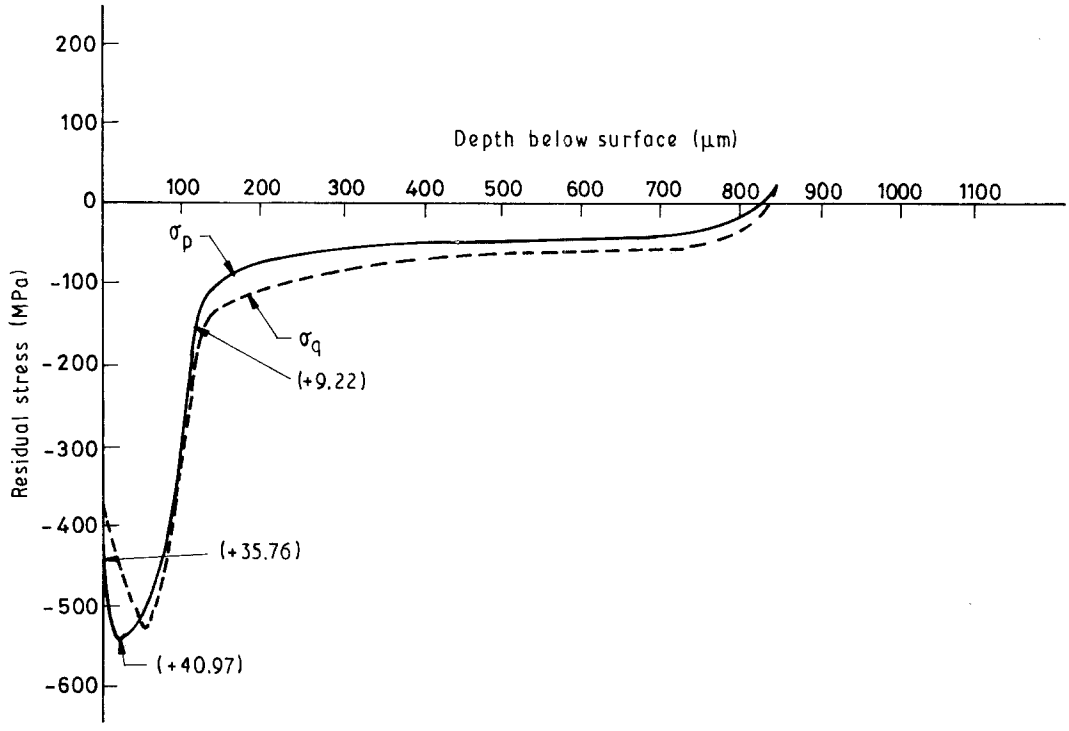

Figure 14 Variation of the principal residual stresses as functions of depth below the specimen surface. IMI-318, machined, polished and wet-glass peened condition. The figures in parentheses indicate the magnitude of the angle β in degrees.

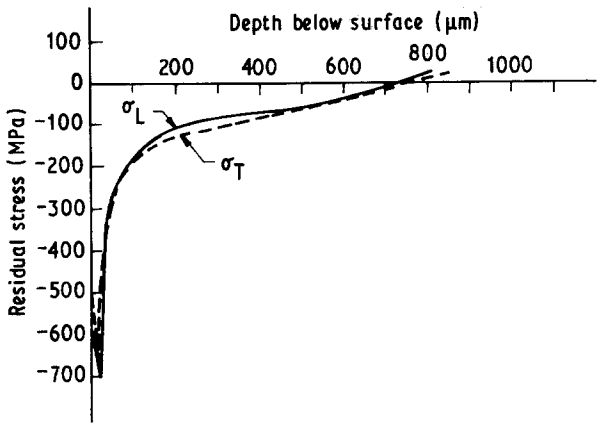

Figure 15 Variation of the longitudinal and transverse residual stresses as functions of depth below the specimen surface. IMI-318, machined, polished and wet-glass peened condition.

their fatigue behaviour differently. The results obtained on this aspect will be reported elsewhere.

4. Conclusions

Based on the present study on the two titanium alloys IMI-685 and IMI-318, the following conclusions could be drawn.

1. In both the alloys, the residual stresses in the machined and polished as well as the machined, polished and shot-peened conditions were compressive.
2. The peak residual stresses present in both the materials following shot peening were not very different.
3. In both the alloys, the principal residual stresses varied both in magnitude and direction with depth below the surface.
4. Mostly, the transverse residual stress, σ_T, was greater than the longitudinal residual stress, σ_L.
5. In both materials the peak residual stresses in the longitudinal direction were about 70%–75% of the respective 0.2% proof stress.
6. The residual stress peak in IMI-685 was found at the surface while in IMI-318 it was present at a subsurface layer. The difference was traced to the lower strain-hardening rate of IMI-685 compared with that of IMI-318.

References

1. A. B. SADAT and J. A. BAILEY, *Exp. Mech.* **21** (1987) 80.
2. J. C. MIDDLETON, *NDT Int.* **20** (1987) 291.
3. G. H. GESSINGER and C. CORTI, Titanium Science and Technology, in "Proceedings of the Fourth International Conference on Titanium", edited by H. Kimura and O. Izumi, (Metallurgical Society of AIME, Warrendale, PA, 1980) p. 1787.
4. A. NICKU-LARI and D. GILLIREAU, *Galvano Organo* **53** (1984) 529.
5. J. O. ALMEN and P. H. BLACK, "Residual Stress and Fatigue in Metals" (McGraw-Hill, New York, 1963) pp. 65–90.
6. S. DENNIS, J. C. CHEVIRIER and G. BECK, in "Titanium Science and Technology, Proceedings of the Third International Conference on Titanium", edited by R. I. Jaffee and H. M. Burte (Plenum Press, New York, 1973) p. 1563.
7. J. MATHAR, *Trans. Amer. Soc. Mech. Eng.* **56** (1934) 249, cited in [10].
8. N. J. RENDLER and I. VIGNESS, in "Proceedings of the Society for Experimental Stress Analysis", SESA Spring Meeting, Detroit, Michigan **23** (May 4–6, 1966) pp. 577–586.
9. N. J. RENDLER and I. VIGNESS, *Exp. Mech.* **6** (1966) 577.
10. "Measurement of Residual Stresses by Blind Hole Drilling Method", Technical Data Bulletin T-403, Measurements Group, Vishay Intertechnology Inc., USA (1977).
11. J. P. SADIFER and G. E. BOWIE, *Exp. Mech.* **18** (1978) 173.
12. A. K. TIEU, *ibid.* **25** (1985) 43.
13. E. PROCTER, "Impact Surface Treatment, Proceedings of the Second International Conference on Impact Treatment Processes", edited by S. A. Meguid (Elsevier Applied Science, London, New York, 1986) pp. 23–30.
14. E. PROCTER and E. M. BEANEY, *Exp. Tech.* **6** (1982) 10.
15. O. VOHRINGER, T. HIRSCH and E. MACHERAUCH, in "Titanium Science and Technology, Proceedings of the Fifth International Conference on Titanium", edited by G. Lutjering, U. Zwicker and W. Bunk, Oberursel, FRG, Vol. 4 (Deutsche Gesellschaft fur Metallkunde, 1984) pp. 2203–10.
16. H. GUECHICHI, L. CASTEX, J. FRELAT and G. INGELBERT, "Impact Surface Treatment, Second International Conference on Impact Treatment Processes", edited by S. A. Meguid (Applied Science, London, New York, 1986) pp. 11–22.
17. S. T. S. Al-HASSANI, in "Proceedings of the Second International Conference on Shot Peening (ICSP-2), edited by H. O. Fuchs (American Shot Peening Society, New Jersey, 1984) pp. 275–82.
18. S. T. S. Al-HASSANI, in "Proceedings of the First International Conference on Shot Peening (ICSP-1)", edited by Nicku-Lari (American Shot Peening Society, New Jersey, 1981) pp. 583–602.
19. H. WOHLFAHRT, in "Proceedings of the Second International Conference on Shot Peening (ICSP-2)", edited by H. O. Fuchs (American Shot Peening Society, New Jersey, 1984) pp. 293–6.
20. P. RAMA RAO Personal communication.

Received 29 July
and accepted 28 November 1991